Can dark energy viscosity be detected with the Euclid survey?

Domenico Sapone[*] and Elisabetta Majerotto[†]

Departamento de Física Teórica and Instituto de Física Teórica, Universidad Autónoma de Madrid IFT-UAM/CSIC,
28049 Cantoblanco, Madrid, Spain

Martin Kunz[‡]

Département de Physique Théorique, Université de Genève, 24 quai Ernest Ansermet, CH-1211 Genève 4, Switzerland
and African Institute for Mathematical Sciences, 6-8 Melrose Road, Muizenberg, 7950 Cape Town, South Africa

Bianca Garilli[§]

IASF-Milano, INAF, Via Bassini 15, I-20133 Milano, Italy

Recent work has demonstrated that it is important to constrain the dynamics of cosmological perturbations, in addition to the evolution of the background, if we want to distinguish among different models of the dark sector. Especially the anisotropic stress of the (possibly effective) dark energy fluid has been shown to be an important discriminator between modified gravity and dark energy models. In this paper we use approximate analytical solutions of the perturbation equations in the presence of viscosity to study how the anisotropic stress affects the weak lensing and galaxy power spectrum. We then forecast how sensitive the photometric and spectroscopic Euclid surveys will be to both the speed of sound and the viscosity of our effective dark energy fluid when using weak lensing tomography and the galaxy power spectrum. We find that Euclid alone can only constrain models with a very small speed of sound and viscosity, while it will need the help of other observables in order to give interesting constraints on models with a sound speed close to one. This conclusion is also supported by the expected Bayes factor between models.

PACS numbers: 98.80.−k, 95.36.+x

I. INTRODUCTION

Since its discovery in 1998 by [1,2], the cause of cosmic acceleration has not been understood, despite all the observational and theoretical efforts in this direction (see e.g. [3–5] and references therein). Ironically, the best explanation from the observational point of view, i.e. a cosmological constant, is not very satisfactory from a theoretical perspective [6]. Among the many alternative possible answers, one proposal is to modify the Einstein equations, either in four dimensions, as in scalar-tensor theories, or in five dimensions, as e.g. in the Dvali-Gabadadze-Porrati model [7], or even in six dimensions [8,9]. All these theories, if rewritten as "effective dark energy" models (simply by moving the additional terms modifying Einstein equations from the geometry side to the matter side of the equations) exhibit a difference with respect to ordinary scalar field dark energy (DE): they possess anisotropic stress.

For this reason, and also because we still do not know what dark energy is really made of, in [10] some of us studied an effective dark energy with anisotropic stress. The latter was modeled as in [11] with the help of a viscosity parameter, in addition to the speed of sound and

equation of state parameters. This parametrization was used first in [12] in relation with dark energy. A further work by [13] analyzed the model with data from the cosmic microwave background (CMB) radiation, large scale structure and type Ia supernovae, and showed that it is hard to constrain both c_s^2 and c_ν^2 and that future data would not improve very much their measurement. In [10] analytical equations describing the cosmological perturbations for this imperfect fluid dark energy were derived, following the lines of a previous paper [14], where the same was done for a model with no viscosity. Other recent work on anisotropic stress can be found in [15].

In this paper we will use these analytical expressions to understand how well the galaxy clustering (GC) and weak lensing (WL) measurements of the Euclid survey[1] [16,17] will be able to constrain the viscosity of the dark energy fluid, together with its speed of sound.

The Euclid survey is a recently selected mission of the ESA Cosmic Vision program, whose launch is planned for 2020. The reason it is particularly apt to constrain imperfect fluid DE (or alternatively modified gravity models) is that it will perform both a photometric survey to measure WL and a spectroscopic survey to measure the galaxy power spectrum (and higher order functions). Both WL and the galaxy power spectrum are able to constrain not only the expansion history of the Universe, which depends

---

[*]domenico.sapone@uam.es
[†]elisabetta.majerotto@uam.es
[‡]martin.kunz@unige.ch
[§]bianca@lambrate.inaf.it

---

[1]http://www.euclid-ec.org/.

on the matter density and the equation of state of DE, but also further observables like the growth of structure. From these additional observables it is possible in principle to measure the speed of sound and the viscosity parameter, and to constrain the evolution of the perturbations. These are precisely the distinctive features of such models.

In this work we will not only forecast the total errors on the model parameters, by using the Fisher matrix formalism, but also analyze separately the different contributions, taking advantage of our analytical formulas. This will allow us to understand better which are the aspects of the WL and of the galaxy power spectrum that have the strongest impact.

We will find that the Euclid survey is marginally able to constrain the viscosity together with the speed of sound, as errors are of the order of 100%. This is due to the complexity of the model and to the smallness of the effects that we wish to detect.

By evaluating the forecasted Bayes' factor we will find moreover that there is (strong) evidence in favor of viscous dark energy, as compared to a dark energy model with the same sound speed but no viscosity, only when the fiducial viscosity and sound speed are very small (but not too small) and when both weak lensing and galaxy clustering are used. In the latter case, decisive evidence in favor of viscous dark energy can be reached if we reduce the maximum viscosity allowed by our flat prior to be less than $\simeq 10^{-1}$; otherwise the Occam's razor effect of the Bayes' factor dominates and disfavors the presence of nonzero viscosity.

The plan of the paper is the following. In Sec. II we briefly describe the model and give the basic equations together with the main formulas found in [10]. We then analyze the different observables and evaluate analytically their sensitivity to the speed of sound and the viscosity parameter in Sec. III. Section IV is devoted to the Fisher matrix forecasts on the errors for our model from the Euclid WL and GC surveys. We analyze our results taking into account the results of the previous section. We forecast the Bayesian evidence using our computed Fisher matrices in Sec. V, and we finally conclude in Sec. VI.

II. APPROXIMATE SOLUTIONS AND GENERAL BEHAVIORS

We start by describing the model we consider: an imperfect fluid dark energy with anisotropic stress. In this section we give the basic equations, defining our notation and presenting the approximate analytical solution to the dark energy perturbation evolution found in [10] (for more details please see the aforementioned paper).

A. Definitions

We consider scalar linear perturbations about a spatially flat Friedmann-Lemaitre-Robertson-Walker Universe, whose line element is, in conformal Newtonian gauge,

$$ds^2 = a^2[-(1 + 2\psi)d\tau^2 + (1 - 2\phi)dx_i dx^i], \quad (1)$$

where a is the scale factor, τ is the conformal time, x_i are the spatial coordinates and ψ and ϕ are the metric perturbations. We take an imperfect fluid dark energy, with constant equation of state w, with speed of sound c_s and with an anisotropic stress component σ. The first order perturbation equations for this fluid are

$$\delta' = 3(1 + w)\phi' - \frac{V}{Ha^2} - 3\frac{1}{a}\left(\frac{\delta p}{\rho} - w\delta\right), \quad (2)$$

$$V' = -(1 - 3w)\frac{V}{a} + \frac{k^2}{Ha^2}\frac{\delta p}{\rho} + (1 + w)\frac{k^2}{Ha^2}\psi$$
$$- (1 + w)\frac{k^2}{Ha^2}\sigma, \quad (3)$$

where δ and V are the density contrast and the velocity perturbation, δp is the pressure perturbation, H is the Hubble function, ρ is the dark energy density and the prime refers to derivatives with respect to the scale factor a. For the evolution of σ, we consider the model proposed by [11]

$$\sigma' + \frac{3}{a}\sigma = \frac{8}{3}\frac{c_v^2}{(1 + w)^2}\frac{V}{a^2 H}, \quad (4)$$

which, for $c_v^2 = 1/3$, recovers the evolution of anisotropic stress for radiation up to the quadrupole and reduces to the case of a classical uncoupled scalar field, which has always $\sigma = 0$, when the viscosity parameter c_v^2 is set to zero.[2] Pressure perturbations are parametrized as

$$\delta p = c_s^2 \rho \delta + \frac{3aH(c_s^2 - c_a^2)}{k^2}\rho V, \quad (5)$$

where the adiabatic speed of sound $c_a^2 \equiv \dot{p}/\dot{\rho} = w$ for a fluid with constant equation of state. Since we focus on late cosmological times, we can approximate H with

$$H^2 = H_0^2[\Omega_{m,0}a^{-3} + (1 - \Omega_{m,0})a^{-3(1+w)}], \quad (6)$$

where $\Omega_{m,0}$ indicates the dark matter density parameter and H_0 is the Hubble parameter today.

To form a complete set of differential equations we add the Poisson equation, derived from the first and second Einstein equations,

$$k^2\phi = -4\pi Ga^2\sum_i \rho_i\left(\delta_i + \frac{3aH}{k^2}V_i\right) = -4\pi Ga^2\sum_i \rho_i\Delta_i \quad (7)$$

(where $\Delta_i \equiv \delta_i + 3aHV_i/k^2$ is the gauge-invariant density perturbation of the ith fluid, the sum runs over all clustering fluids and G is the Newton constant), and the fourth Einstein equation,

---

[2] In the case where $c_v^2 = 0$ the viscosity decays as $\sigma \sim a^{-3}$ even if it is initially nonzero and vanishes indeed rapidly.

$$k^2(\phi - \psi) = 12\pi G a^2 (1 + w)\rho\sigma \tag{8}$$

$$= \frac{9}{2}H_0^2(1 - \Omega_{m,0})a^{-(1+3w)}(1 + w)\sigma$$

$$\equiv B(a)\sigma. \tag{9}$$

B. Analytical solutions for dark energy perturbations

In the aforementioned approximations and with assuming matter domination we have found in [10] the following analytical solutions for δ, V and σ:

$$\delta = \frac{3(1 + w)^2}{3c_s^2(1 + w) + 8(c_s^2 - w)c_v^2} \frac{\phi_0}{k^2}, \tag{10}$$

$$V = -\frac{9(1 + w)^2(c_s^2 - w)}{3c_s^2(1 + w) + 8c_v^2(c_s^2 - w)}H_0\sqrt{\Omega_m}\frac{\phi_0}{\sqrt{a}k^2},$$

$$= -3aH(c_s^2 - w)\delta, \tag{11}$$

$$\sigma = -\frac{8c_v^2(c_s^2 - w)}{3c_s^2(1 + w) + 8(c_s^2 - w)c_v^2} \frac{\phi_0}{k^2}, \tag{12}$$

where the constant ϕ_0 is defined from the relation $k^2\phi \simeq -\phi_0$, which is valid strictly only during matter domination and while neglecting dark energy perturbations.

As already shown in [10], modes above the sound horizon at early times are effectively uncoupled from the anisotropic stress, since the term on the right hand side of Eq. (4) is small compared to the terms on the left hand side. Here dark energy perturbations follow the standard evolution for $c_v^2 = 0$, which was found in [14]

$$\delta = (1 + w)\frac{\phi_0}{c_s^2 k^2}, \tag{13}$$

$$V = -\frac{3(1 + w)(c_s^2 - w)H_0\sqrt{\Omega_{m,0}}}{c_s^2 k^2}a^{-1/2}, \tag{14}$$

$$\sigma = 0. \tag{15}$$

We remark that, as can be seen by comparing Eqs. (10) and (13), the damping introduced by viscosity is stronger by a factor $(1 + w)$ with respect to the standard case of isotropic dark energy. The Eqs. (10)–(12) can be rewritten in terms of an effective sound speed [10]

$$c_{\text{eff}}^2 = c_s^2 + \frac{8}{3}c_v^2 \frac{c_s^2 - w}{1 + w}. \tag{16}$$

This means that the important quantity determining the growth of the dark energy perturbations is a combination of the sound speed and the viscosity. These have a similar damping effect on density and velocity perturbations.

We also point out that while normally the case $w = -1$ represents a singularity for dark energy perturbations, the situation is less clear when anisotropic stress is present.

In general it is enough to keep $(1 + w)\sigma$ finite as $w \rightarrow -1$. In addition, although the source term of Eq. (4) appears singular in this limit, we can see from Eq. (11) that V decays $\propto (1 + w)^2$ for our model and so the term does not actually diverge.

III. OBSERVABLE EFFECTS OF VISCOSITY ON GALAXY CLUSTERING AND WEAK LENSING

Once we have shown the analytic expression of density and velocity perturbations and of the anisotropic stress, let us see how these enter our observables. In particular, in this section we evaluate the impact of viscosity on galaxy clustering and weak lensing maps, in order to understand what to expect from the error forecasts. To do this we look at the derivatives of our observables with respect to the parameters c_s^2 and c_v^2. These derivatives will appear in the Fisher matrix computation: the larger the derivative, the stronger the dependence of our observable from the analyzed parameter, and the smaller the forecasted error. We analyze separately each different component characterizing these observables and evaluate analytically its impact in the total derivative, with the help of the analytical parameters introduced in [18]: the clustering parameter Q and the anisotropy parameter η.

A. Parametrizing dark energy perturbations

First of all, we shortly describe our parameters, which will help us understand the behavior of our observables in the presence of a non-null c_v^2. The clustering parameter $Q \equiv 1 + \rho\Delta/(\rho_m\Delta_m)$ (where Δ, Δ_m are gauge-invariant comoving density perturbations), quantifying the size of the dark energy perturbations compared to the matter perturbations (and hence to the total perturbations, given that dark energy perturbations are much smaller than matter ones), parametrizes the deviation from a purely matter-dominated Newtonian potential. In the presence of viscosity we have obtained [10]

$$Q - 1 = \frac{1 - \Omega_{m,0}}{\Omega_{m,0}}(1 + w)\frac{a^{-3w}}{1 - 3w + \frac{2k^2 a}{3H_0^2\Omega_{m,0}}c_{\text{eff}}^2}$$

$$= Q_0 \frac{a^{-3w}}{1 + \alpha a}, \tag{17}$$

where $\alpha = 2k^2 c_{\text{eff}}^2 / [(3H_0^2\Omega_{m,0})(1 - 3w)]$, $Q_0 = (1 + w) \times (1 - \Omega_{m,0})/[\Omega_{m,0}(1 - 3w)]$ and c_{eff}^2 is given by Eq. (16). Notice that, as explained in [10], Eq. (17) is valid also for $c_s^2 = c_v^2 = 0$.

As regards the anisotropy parameter, this is defined as

$$\eta \equiv \frac{\psi}{\phi} - 1. \tag{18}$$

It is zero in the case of standard general relativity with nonanisotropic fluids because then the two metric perturbations ϕ and ψ are equal. When anisotropic stress is present instead, ϕ and ψ are different. In our case η is indeed non-null and given by

$$\eta = -\frac{9}{2} H_0^2 (1 - \Omega_{m,0})(1+w) \frac{a^{-1-3w}}{k^2 Q} \left(1 - \frac{c_s^2}{c_{\text{eff}}^2}\right). \quad (19)$$

Having established the dependence of Q and η on c_s^2 and c_v^2, we evaluate then how the main "ingredients" of the WL power spectrum and galaxy power spectrum, i.e. the matter power spectrum, the redshift space distortions and the weak lensing potential, depend on Q and η, and hence on the speed of sound and the viscosity parameter.

B. The dark matter power spectrum

The linear matter power spectrum $P_m(k, a)$ can be expressed as the product of today's $P_m(k)$ and its redshift evolution $G(a, k)$. Today's matter power spectrum $P_m(k)$ is affected by dark energy perturbations, and hence by c_s^2 and c_v^2, through a linear dependence on Q. This is because the matter density contrast δ_m is sourced by the gravitational potential ϕ, which is in turn modified by the presence of δ. The Poisson equation (7) can indeed be expressed as

$$k^2 \phi = -4\pi G a^2 Q \rho_m \Delta_m. \quad (20)$$

Hence, we can try to assess how sensitive the matter power spectrum today is to changes of the sound speed and the viscosity, by computing the derivatives of Q with respect to c_s^2 and c_v^2:

$$\frac{\partial Q}{\partial c_s^2} = -\frac{\alpha a}{1 + \alpha a}(Q - 1)\frac{c_{\text{eff}}^2 - w}{c_{\text{eff}}^2(c_s^2 - w)}, \quad (21)$$

$$\frac{\partial Q}{\partial c_v^2} = -\frac{\alpha a}{1 + \alpha a}(Q - 1)\frac{c_{\text{eff}}^2 - c_s^2}{c_{\text{eff}}^2 c_v^2}. \quad (22)$$

The derivatives of Q with respect to c_s^2 and c_v^2 are shown in Fig. 1 (red solid lines). In Fig. 2 we then show how the derivatives of Q with respect to c_s^2 vary when changing the fiducial model: on the left panels we vary the fiducial c_s^2, which takes the values $c_s^2 = 10^{-6}$, 10^{-5} and 10^{-4} and c_v^2 is fixed to 10^{-4}, while on the right panels $c_v^2 = 10^{-6}$, 10^{-5} and 10^{-4} and $c_s^2 = 10^{-4}$ (we always use units where the speed of light is $c = 1$). Our first consideration looking at the figure is that reducing the fiducial value of c_s^2 or c_v^2 improves the sensitivity of Q to them, but not indefinitely: the smaller c_s^2 or c_v^2, the smaller the improvement. Second, we notice that Q is a factor of ~ 10 more sensitive to c_v^2 than c_s^2 (compare corresponding top and bottom panels). The reason for this is to be found in the dependence of Q on c_s^2 and c_v^2 through c_{eff}^2: in its expression a factor of ~ 10 multiplies c_v^2, so that the sensitivity of c_{eff}^2 to c_v^2 is better by such a factor than that to c_s^2.
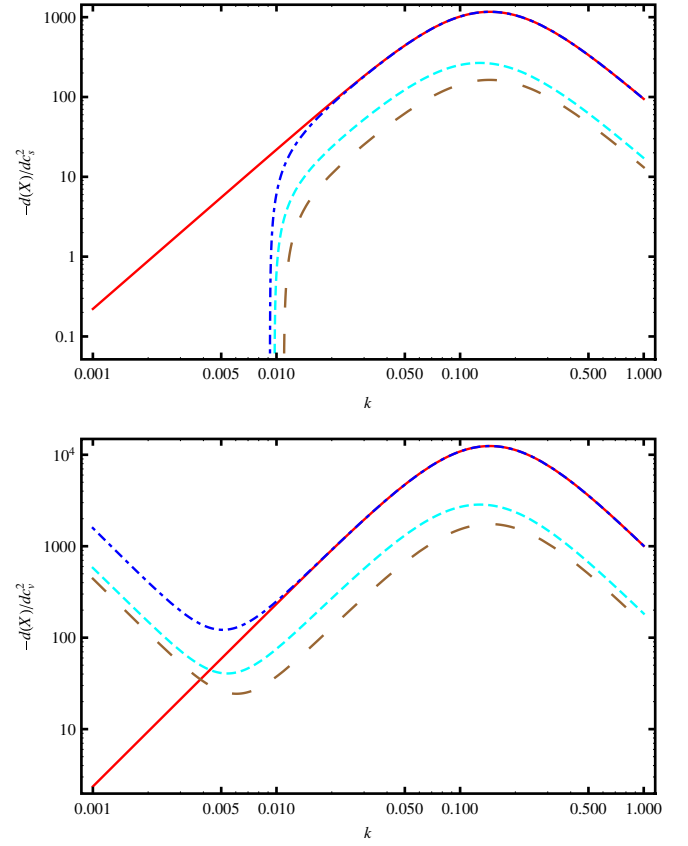

FIG. 1 (color online). Here we show the sensitivity of the parameters entering the WL and GC observables to the sound speed c_s^2 and the anisotropy parameter c_v^2. Plotted are the derivatives of $Q(a, k)$ (red solid lines), $\Sigma(a, k)$ (blue dot-dashed lines), $G(a, k)$ (cyan short-dashed lines), and $f(a, k)$ (brown long-dashed lines) with respect to c_s^2 (top panel) and to c_v^2 (bottom panel), as a function of the wave number k in units of h/Mpc. The viscosity term is set to $c_v^2 = 10^{-6}$ and the sound speed to $c_s^2 = 10^{-6}$. We can see that the most sensitive parameters are Σ and Q and that these two parameters are degenerate (i.e. have the same amplitude and shape) if k is larger than $\sim 0.1 h/\text{Mpc}$.

C. The growth factor

The growth factor, characterizing the change of the matter power spectrum with respect to today's shape and amplitude, is given by

$$G(k, a) = \int_{a_0}^{a} \frac{f(a', k)}{a'} da', \quad (23)$$

where a_0 is today's scale factor, the growth rate f can be expressed as

$$f(a, k) = \Omega_m(z)^{\gamma(k,z)}, \quad (24)$$

and the growth index $\gamma(k, z)$ can be written in terms of Q and η [19]:
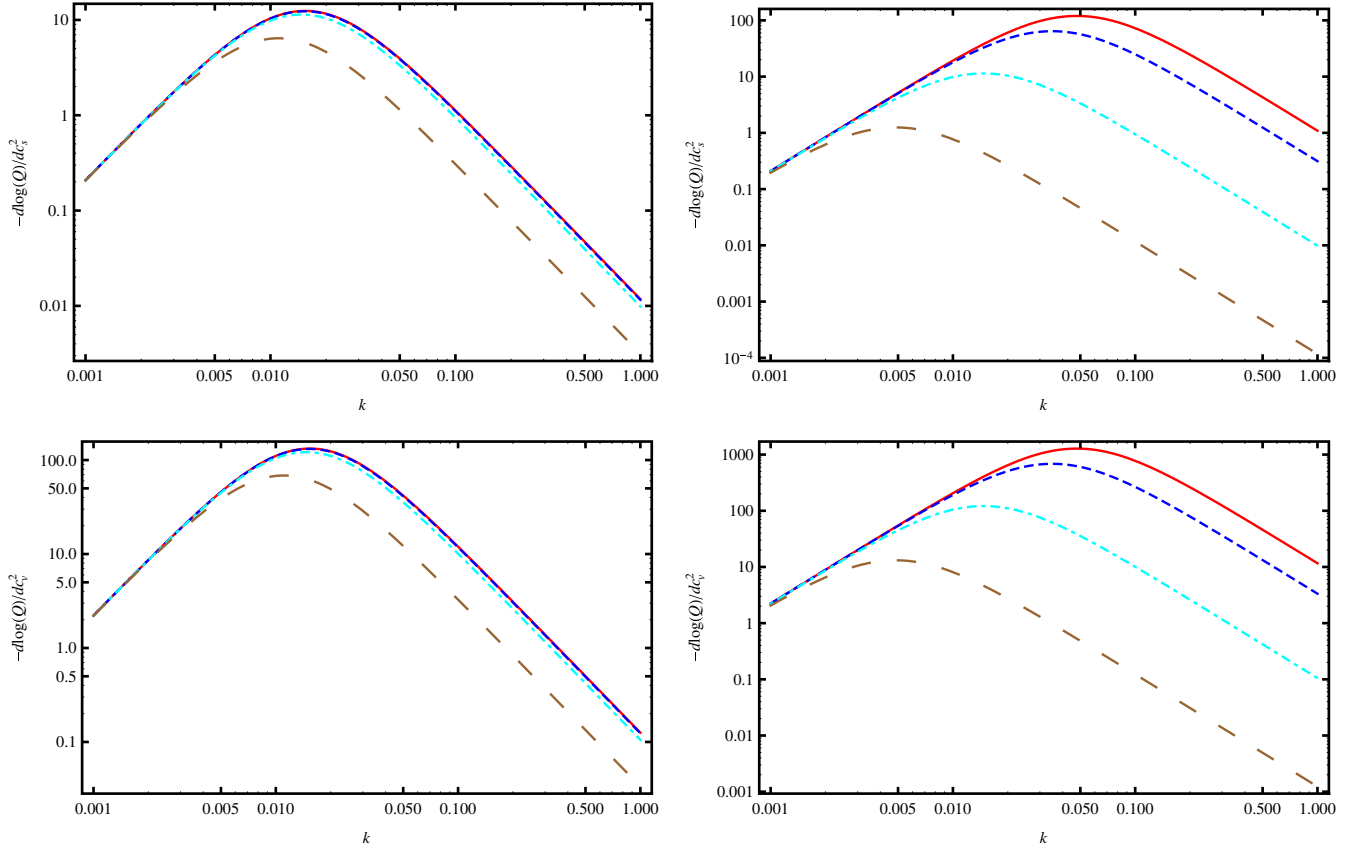
FIG. 2 (color online). Here we show how the sensitivity of Q to the sound speed c_s^2 and the viscosity parameter c_v^2 depend on the amplitude of c_s^2 (left panels) and c_v^2 (right panel). We plot the derivative of the logarithm of $Q(a, k)$ with respect to the sound speed c_s^2 (top panels) and to the viscosity parameter c_v^2 (bottom panels) as a function of the wave number k in units of h/Mpc. On the left panels, we fix the viscosity term $c_v^2 = 10^{-6}$ and the sound speed c_s^2 takes values 10^{-3}, 10^{-4}, 10^{-5} and 10^{-6}, brown long dashed, cyan dot-dashed, blue dashed and red solid lines, respectively. On the right panels, we fix the viscosity term $c_s^2 = 10^{-6}$ and the sound speed c_v^2 takes values 10^{-3}, 10^{-4}, 10^{-5} and 10^{-6}, brown long dashed, cyan dot-dashed, blue dashed and red solid lines, respectively. It can be seen that reducing the value of c_s^2 or c_v^2 improves the sensitivity of Q to them, but the smaller c_s^2 or c_v^2, the smaller the improvement. We also see that Q is a factor of ~10 more sensitive to c_v^2 than c_s^2 (compare corresponding top and bottom panels). This is because Q depends on sound speed and viscosity through c_{eff}^2, in whose expression a factor of ~10 multiplies c_v^2 while c_s^2 is multiplied by a factor of 1.

$$\gamma = \frac{3(1 - w - A(Q, \eta))}{5 - 6w}, \qquad (25)$$

with

$$A(Q, \eta) = \frac{(1 + \eta)Q - 1}{1 - \Omega_m(a)}. \qquad (26)$$

Using Eqs. (25) and (26) we can compute the derivatives $\partial G/\partial c_s^2$, $\partial G/\partial c_v^2$ as follows:

$$\frac{\partial G}{\partial c_s^2} = -G \frac{3Q_0}{5 - 6w} \frac{c_{\text{eff}}^2 - c_s^2}{c_{\text{eff}}^2(c_s^2 - w)}$$
$$\times \int_{a_0}^{a} \left[\frac{3w}{\alpha} x^{-3w-2} + \alpha \frac{c_{\text{eff}}^2 - w}{c_{\text{eff}}^2 - c_s^2} \frac{x^{-3w}}{(1 + \alpha x)^2} \right] dx,$$
$$(27)$$

$$\frac{\partial G}{\partial c_v^2} = -G \frac{3Q_0}{5 - 6w} \frac{c_{\text{eff}}^2 - c_s^2}{c_{\text{eff}}^2 c_v^2}$$
$$\times \int_{a_0}^{a} \left[\frac{3c_s^2}{\alpha} x^{-3w-2} + \alpha \frac{x^{-3w}}{(1 + \alpha x)^2} \right] dx. \qquad (28)$$

These are shown in Fig. 1 (cyan short-dashed line). Comparing the derivatives with respect to c_s^2 and c_v^2 of G with those of Q we notice that the former are smaller than the latter, implying a smaller sensitivity of the latter to the sound speed and the viscosity. As also explained in [20], this is because G depends on the integral of Q: the growth factor is not probing the deviation of Q from unity, but rather how Q evolves with time.

D. The weak lensing potential

In WL experiments, the important quantity is the lensing potential $\Phi = \phi + \psi$. As regards ϕ, the Poisson equation

couples it to the dark energy contrast, and we expressed the influence of the latter through the parameter Q; see Eq. (20). The potential ψ instead is related to the aniso-tropic stress, and the parameter connecting it to ϕ is η, as in Eq. (18). Hence, using Eqs. (20) and (18) we find the following for Φ:

$$k^2\Phi = -8\pi G a^2 \left(1 + \frac{1}{2}\eta\right) Q\rho_m\Delta_m. \qquad (29)$$

The resulting quantity is therefore a combination of the anisotropic stress and the dark energy density contrast,

$$\Sigma = \left(1 + \frac{1}{2}\eta\right)Q, \qquad (30)$$

and it represents the deviation of the WL potential from the standard case of no dark energy perturbations. We can compute now the derivatives of Σ with respect to the sound speed c_s^2 and the viscosity term c_v^2:

$$\frac{\partial\Sigma}{\partial c_s^2} = -(Q-1)\left\{\frac{\alpha a}{1+\alpha a}\frac{1}{c_{\mathrm{eff}}^2}\left[1 + \frac{8}{3}\frac{c_v^2}{1+w}\right] \right.$$
$$\left. + 4\frac{1+\alpha a}{\alpha a}\frac{c_v^2}{c_{\mathrm{eff}}^2}\frac{w}{1+w}\right\} \qquad (31)$$

$$\frac{\partial\Sigma}{\partial c_v^2} = -(Q-1)4\frac{c_s^2-w}{1+w}\left\{\frac{\alpha a}{1+\alpha a}\frac{1}{c_{\mathrm{eff}}^2}\frac{2}{3} + \frac{1+\alpha a}{\alpha a}\frac{c_s^2}{c_{\mathrm{eff}}^2}\right\}, \qquad (32)$$

and plot them in Fig. 1 together with the other derivatives. We clearly see that at scales smaller than $k \sim 0.01 h/\mathrm{Mpc}$ the derivatives with respect to c_s^2 or c_v^2 of Σ have the same amplitude and shape as those of Q. Looking at the expression of $\partial\Sigma/\partial c_s^2$, $\partial\Sigma/\partial c_v^2$, Eqs. (31) and (32), this means that η only plays a role at very large scales, while its contribution is very small at all other scales. This can also be seen in the expression for η, Eq. (19), which contains a factor $(Ha/k)^2$ relative to $Q-1$, Eq. (17), and so is sup-pressed on subhorizon scales. A confirmation of this can be found in Fig. 3, which shows the evolution with k of the derivatives of η, which are much smaller than those of Q. We also notice, comparing the upper to the lower panel of Fig. 1 that for small values of the speed of sound and the viscosity (as those selected to produce the plot), the derivatives with respect to c_s^2 are identical in shape to those with respect to c_v^2, if we consider smaller scales.

E. Redshift space distortions

   Galaxy redshift surveys do not directly observe the total matter distribution: they produce a three-dimensional (3D) map of the galaxy distribution, where the information on the radial distance to each galaxy is obtained through the measured galaxy redshift. Because of the galaxy peculiar velocities, the redshift map is distorted with respect to the real space map. Such redshift space distortion (RSD) was
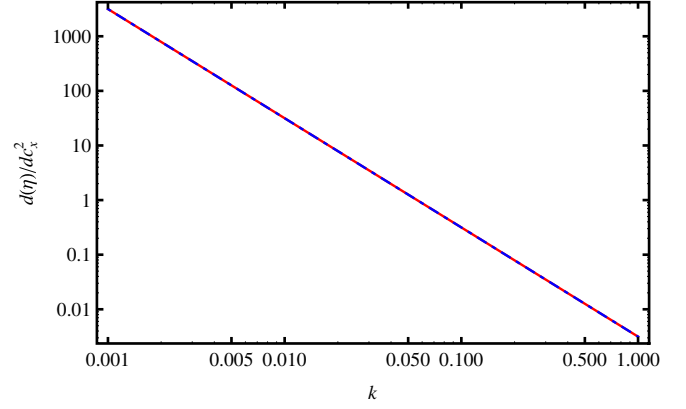

FIG. 3 (color online).   Here we show the sensitivity of the anisotropy parameter η to the sound speed c_s^2 and viscosity parameter c_v^2. Derivatives of $\eta(a,k)$ with respect to the sound speed c_s^2 (solid red line) and the viscosity parameter c_v^2 (blue dot-dashed line) are shown as a function of the wave number k in units of h/Mpc. Here the fiducial viscosity term is $c_v^2 = 10^{-6}$ and the fiducial sound speed is $c_s^2 = 10^{-6}$. By comparing the size of these derivatives to that of the corresponding derivatives of Q of Fig. 1 we notice that the first are much smaller than the second when $k > 0.01 h/\mathrm{Mpc}$, so that their contribution to the derivatives of Σ (related to the WL potential) is very small at smaller scales.

first described by [21], who modeled it through a factor $(1 + (f(k,z)/b)\mu^2)^2$ multiplying the matter power spec-trum, where f is the growth rate [see Eq. (24)], b is the bias factor relating the amplitude of the galaxy power spectrum to the matter power spectrum, and μ is the cosine of the component of k parallel to the line of sight.

   For this reason, we evaluate here the sensitivity of f to sound speed and viscosity parameter by computing the derivatives of f with respect to c_s^2 and c_v^2. These are given by $\partial f/\partial c_s^2 = f\ln\Omega_m(a)\partial\gamma/\partial c_s^2$ (and equivalently for c_v^2). Since the main dependence on viscosity and speed of sound will come from the term $\partial\gamma/\partial c_s^2$ (given that the term f will be close to 1 during matter domination), we only show here the analytical derivatives of γ:

$$\frac{\partial\gamma}{\partial c_s^2} = \frac{3(Q-1)}{(5-6w)(1-\Omega_m(a))}\frac{c_{\mathrm{eff}}^2 - c_s^2}{c_{\mathrm{eff}}^2(c_s^2-w)}$$
$$\times\left[3w\frac{1+\alpha a}{\alpha a} + \frac{c_{\mathrm{eff}}^2-w}{c_{\mathrm{eff}}^2-c_s^2}\frac{\alpha a}{1+\alpha a}\right], \quad (33)$$

$$\frac{\partial\gamma}{\partial c_v^2} = \frac{3(Q-1)}{(5-6w)(1-\Omega_m(a))}\frac{c_{\mathrm{eff}}^2-c_s^2}{c_{\mathrm{eff}}^2 c_v^2}$$
$$\times\left[3c_s^2\frac{1+\alpha a}{\alpha a} + \frac{\alpha a}{1+\alpha a}\right]. \qquad (34)$$

The logarithm of the derivatives of the Kaiser term with respect to c_s^2 and c_v^2 (integrated over the angle μ) are shown as well in Fig. 1. Their shape is very similar to that of the derivatives of G and of Σ but they always have a

smaller size than them, which means that the contribution of the RSD in the detection of c_s^2 and c_v^2 should not be very important.

F. Comparison of galaxy power spectrum and weak lensing potential

We want now to identify exactly the quantities entering the galaxy power spectrum and the WL power spectrum, in order to understand which of them is more sensitive to the sound speed and the viscosity parameter.

Let us start with the former: it will depend on the matter power spectrum and on the RSD factor; hence the relevant parameters for detecting DE perturbations will be Q [see Eq. (20)] and the growth factor G, related to the matter power spectrum today and its evolution with time, respectively, and the growth rate f, detectable through the RSD term. If we consider the WL power spectrum, this will again depend on the matter power spectrum, hence on Q and G, and also on the difference between the two gravitational potentials, proportional to Σ, as from Eq. (29). We see from Fig. 1 that the contribution from f is the smallest, and that the sensitivity to variations in c_s^2 and c_v^2 of G is slightly lower than that of Σ and Q. This means that in principle WL surveys, measuring Σ, should be slightly more sensitive than galaxy redshift surveys, which measure f.[3] However, other considerations have to be made. Derivatives of Σ and Q differ in shape and amplitude only in the region of very large scales. As this region is not probed by WL measurements (because of the size of the survey and of the projection on the sphere), constraints to c_s^2 and c_v^2 will be degenerate: it will be very difficult to separately measure them.

Moreover, the actual result will depend also importantly on the properties of the single surveys, "weighted" by the sensitivities discussed above.

IV. FORECASTS FOR THE EUCLID SURVEY

With the help of the sensitivity of our observables to c_s^2 and c_v^2 that have evaluated analytically, we can now forecast the actual precision with which the Euclid WL and GC surveys will be able to measure these parameters. As already mentioned, Euclid [17] is a medium-size mission of the ESA Cosmic Vision program, recently adopted for implementation, whose launch is planned for 2020. It will perform two surveys: a photometric survey in the visible and in three near-infrared bands, to measure weak gravitational lensing maps by imaging ~1.5 billion galaxies, and a spectroscopic slitless survey of ~65 million galaxies. Both surveys will be able to constrain both the

expansion and growth history of the Universe and will cover a total area of 15,000 square deg.

Our fiducial Euclid survey follows the specifications that can be found in the Euclid Definition Study Report (also called Red Book) [17], and corresponds to the most up-to-date simulations of Euclid's performance.

As a fiducial model for our Fisher analysis we choose the WMAP-7 flat ΛCDM cosmology, as also used in the Euclid Red Book [17], with the exception of the value of w, which we set to $w = -0.8$. This means that we have $\Omega_{m,0}h^2 = 0.13$, $\Omega_{b,0}h^2 = 0.0226$, $\Omega_\Lambda = 1 - \Omega_{m,0} = 0.73$, $H_0 = 71$, $n_s = 0.96$ (where n_s is the scalar spectral index). The matter power spectrum was computed using CAMB[4] [23].

A. Weak lensing

We start by investigating the sensitivity of the Euclid WL survey to the dark energy parameters. We proceed as in [18,20], the only difference here being that we add the contribution of the anisotropic stress.

Following Eqs. (29) and (30) we can evaluate the convergence WL power spectrum (which in the linear regime is equal to the ellipticity power spectrum): this is a linear function of the matter power spectrum convoluted with the lensing properties of space. For a ΛCDM cosmology it can be written as

$$P_{ij}(\ell) = H_0^4 \int_0^\infty \frac{dz}{H(z)} W_i(z) W_j(z) P_{nl}\left[P_l\left(\frac{H_0\ell}{r(z)}, z\right) \right], \quad (35)$$

where ℓ is the multipole number, W_i's are the window functions, and $P_{nl}[P_l(k, z)]$ is the nonlinear power spectrum at redshift z obtained correcting the linear matter power spectrum $P_l(k, z)$; see [18] for more details.

When dark energy perturbations come into play, the former gets modified. There is no easy way to modify the convergence power spectrum when we consider the nonlinear scales, because we need to evaluate the WL power spectrum, i.e. $\langle\Phi^2\rangle$, which only at linear scales is simply proportional to $\Sigma^2\langle\Delta_m^2\rangle$. If we consider nonlinear scales, the above expression is no longer strictly valid because Σ is a first order quantity. In practice, we would need to convolute the modified linear matter power spectrum $P_{nl}(\Sigma^2 P(k))$. We instead compute $\Sigma^2 P_{nl}(P(k))$.[5]

---

[3]To be precise, as pointed out e.g. in [22], the quantities that can really be observed are the combinations f/b and $f + f'/f$ and not f itself. Since the sensitivity of f to c_s^2 and c_v^2 is very small, and since b is of order unity, this does not change our conclusions.

[4]http://camb.info.

[5]The reason for this is that to include the effect of dark energy perturbations in the nonlinear power spectrum we cannot make use of the analytic expression of P_{nl}, which is designed for the case of absence of dark energy perturbations. So if we want to take the latter into account, we need to solve the Boltzmann equations, hence use CAMB, which does not, however, compute $P_{nl}(\Sigma^2 P_l)$ but only $P_{nl}(P_l)$. Therefore we decided to make the aforementioned approximation $P_{nl}(\Sigma^2 P_l) \sim \Sigma^2 P_{nl}(P_l)$, although it is unclear how large is the error we commit when making it.

The *modified* convergence power spectrum is then

$$P_{ij}(\ell) = H_0^4 \int_0^\infty \frac{\mathrm{d}z}{H(z)} W_i(z) W_j(z) \Sigma^2 P_{nl}\left[P_l\left(\frac{H_0\ell}{r(z)}, z\right)\right]. \quad (36)$$

The Fisher matrix for WL is then given by

$$F_{\alpha\beta} = f_{\mathrm{sky}} \sum_\ell \frac{(2\ell+1)\Delta\ell}{2} \partial(P_{ij})_{,\alpha} C_{jk}^{-1} \partial(P_{km})_{,\beta} C_{mi}^{-1}, \quad (37)$$

where f_{sky} is the observed fraction of the sky, the partial derivatives represent $\partial/\partial\theta_\alpha$, the corresponding cosmological parameters θ_α are shown in Table I and

$$C_{jk} = P_{jk} + \delta_{jk} \frac{\langle\gamma_{\mathrm{int}}^{1/2}\rangle}{n_j}, \quad (38)$$

where γ_{int} is the rms intrinsic shear (here we assume $\langle\gamma_{\mathrm{int}}^{1/2}\rangle = 0.22$ [24]) and n_j is the number of galaxies per steradians belonging to the jth bin.

We compute the Fisher matrix for three fiducial models: the case where $c_s^2 = c_v^2 = 10^{-6}$, $c_s^2 = c_v^2 = 10^{-4}$ and $c_s^2 = 1$, $c_v^2 = 0$. The remaining parameters that we allow to vary here are $\Omega_{m,0}h^2$, $\Omega_b h^2$, n_s, $\Omega_{m,0}$, w_0.

In the WL survey the redshift range covered is $0 < z < 2.5$, which we divide into 10 bins chosen such as to contain an approximately equal number of galaxies each.

Figure 4 shows the 1, 2 and 3σ Fisher ellipses for the parameters c_s^2 and c_v^2. As we can see, the 1σ errors are of the order of 10,000% on c_s^2 and of 1000% on c_v^2, but more importantly we immediately notice that there is a very strong degeneracy between c_s^2 and c_v^2.

To explain it, we should first remember that the parameters measured by WL are Q, Σ and G but as shown in Fig. 1, the contribution of the growth factor G to the total derivatives is small; hence the relevant parameters are Q and Σ. Let us look at the derivative of the weak lensing parameter Σ with respect to the viscosity term c_v^2, i.e. Eq. (32), and rewrite it as

TABLE I. Cosmological parameters (for the derivatives) for galaxy power spectrum and WL survey.

	Parameters	$P(k)$	WL
1	Total matter density	$\Omega_{m_0}h^2$	$\Omega_{m_0}h^2$
2	Total baryon density	$\Omega_{b_0}h^2$	$\Omega_{b_0}h^2$
3	Spectral index	n_s	n_s
4	Matter density today	Ω_{m_0}	Ω_{m_0}
5	Equation of state parameter	w_0	w_0
6	Sound speed	c_s^2	c_s^2
7	Viscosity parameter	c_v^2	c_v^2
	For each redshift bin		
8	Shot noise	P_s	

$$\frac{\partial\Sigma}{\partial c_v^2} = -Q_0 a^{-3w} \frac{\alpha a}{(1+\alpha a)^2} \frac{1}{c_{\mathrm{eff}}^2} \frac{8}{3} \frac{c_s^2 - w}{1+w}$$
$$+ \frac{1+\alpha a}{\alpha a} \frac{c_s^2}{c_{\mathrm{eff}}^2} 4 \frac{c_s^2 - w}{1+w}, \quad (39)$$

where the first term on the right hand side is simply the derivative of Q with respect to c_v^2 [see Eq. (22)], while the second term is directly connected to the anisotropic stress, and hence to η. It can be seen that for small enough values of c_s^2 and c_v^2, $\alpha a \propto k^2 a$ is always smaller than 1. In particular, when k tends to zero, the second term dominates and grows, as can be seen from Figs. 1 and 3. Instead, when k grows, and while $(1 + \alpha a) \sim 1$, the first term behaves like k^2 and the second like $1/k^2$, so that the first term dominates.

Therefore, when the sound speed and the viscosity terms are small enough, for example when $c_s^2 = c_v^2 = 10^{-6}$, then the first term on the right hand side of Eq. (39) is the dominant component—this is due to the relative increase of the dark energy perturbations, which is measured by Q. When we increase the value of c_s^2, the first term in Eq. (39) starts to get smaller; as $\alpha a \sim 1$, the two terms become comparable in size, and they contribute equally to the total derivative.

We can show this numerically: for modes below the causal horizon with $k = 200 H_0$, and assuming $c_s^2 = c_v^2 = 10^{-6}$, the first term in Eq. (39) is of the order of 10^4, whereas the second term is of order unity. If we set $c_s^2 = 1$ and $c_v^2 = 0$ instead, we have that both terms become of the order of 10^{-4}.

So if both values of c_s^2 and c_v^2 are very small, the largest contribution in the derivative of Σ comes from the term proportional to the derivative of Q. Since, as explained earlier, the two parameters measured by WL that contribute most strongly to the determination of c_s^2 and c_v^2 are Q and Σ, and since their derivatives with respect to c_s^2 are proportional to those with respect to c_v^2 for small enough scales, given that here they carry *almost* the same information, these parameters will be *almost* degenerate. This is reflected by the top panel (and more mildly by the middle one) of Fig. 4 and by our WL Fisher matrix, which will be *almost* singular (see also [25] on this topic).

Moreover, we can understand the degeneracy by looking again at the first term on the right hand side of Eq. (39). When c_s^2 is very small, the term $c_s^2 - w \simeq -w$ so that all dependence on the speed of sound and viscosity parameter comes from c_{eff}^2. The degeneracy direction will therefore be that of constant c_{eff}^2, as can easily be verified from Fig. 4. An important consequence of this is that the inversion of the matrix will be unstable and the results will not be reliable, and the reason is that our data are not able to constrain the two parameters c_s^2 and c_v^2 at the same time but only a combination of them. This implies that the top panel of Fig. 4 cannot be considered a reliable result apart from showing us the existence of a strong degeneracy between viscosity and speed of sound. This is also confirmed by
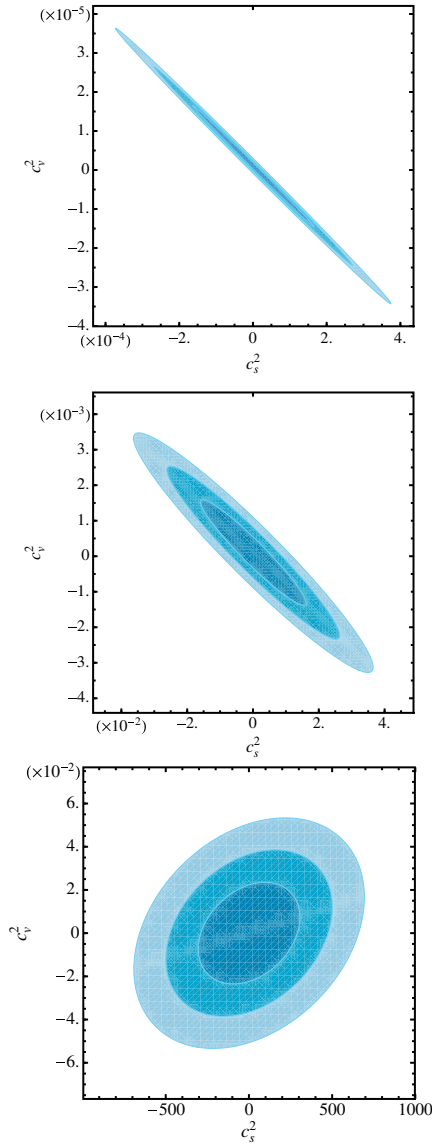
FIG. 4 (color online). Here we plot the forecasted errors on sound speed c_s^2 and viscosity parameter c_v^2 from the Euclid WL survey. Shown are the 1, 2 and 3σ Fisher ellipses for the parameters c_s^2 and c_v^2. The top panel corresponds to the fiducial $c_s^2 = c_v^2 = 10^{-6}$, the central panel to $c_s^2 = c_v^2 = 10^{-4}$ and the bottom one to the case $c_s^2 = 1$ and $c_v^2 = 10^{-6}$. In the case of the top and central panels, a very strong degeneracy between c_s^2 and c_v^2 can be seen. This is because when c_s^2 and c_v^2 are very small, the contributions from Σ and Q are very similar and both constrain $c_{\rm eff}^2$ rather than different combinations of c_s^2 and c_v^2.

comparing the elements of the relative Fisher matrix to the corresponding one for galaxy clustering. The middle panel is slightly closer to be reliable, while the bottom panel, where the fiducial values are $c_s^2 = 1$ and $c_v^2 = 0$, is reliable because c_s^2 is large enough to break the degeneracy between c_s^2 and c_v^2.

We summarize our results in Table II, where we indicate the fully marginalized errors on c_s^2 and c_v^2. Let us recall again the caveat previously explained: errors associated

TABLE II.   Relative errors on the parameters c_s^2 and c_v^2 from the Euclid WL survey. For the case $c_v^2 = 0$ the absolute error $\sigma_{c_v^2}$ is given.

		WL	
c_s^2	c_v^2	$\sigma_{c_s^2}/c_s^2$	$\sigma_{c_v^2}/c_v^2$
10^{-6}	10^{-6}	109	10.3
10^{-4}	10^{-4}	106	9.81
1	0	201	$\sigma_{c_v^2} = 1.55 \times 10^{-2}$

with the fiducial models $c_s^2 = c_v^2 = 10^{-6}$ ($c_s^2 = c_v^2 = 10^{-4}$) are strongly (considerably) unreliable as they have been computed from an almost degenerate Fisher matrix. We list them here only for completeness.

Before closing this section, let us look again at Eq. (37). The summation over ℓ has been stopped at the default "very optimistic" $\ell_{\rm max} = 5000$ used also in [17], which falls into deeply nonlinear scales (but regards the matter power spectrum only and is considered to be more reliable in the standard ΛCDM case). This amounts to believing that we will have an adequate description of this regime for the anisotropic stress model by the time the Euclid satellite will be launched. Moreover, our results depend also on the assumptions made to compute the nonlinear power spectrum (we use CAMB's implementation of the halo model and multiply it by Σ to get the final power spectrum). We can now make two considerations: first, the nonlinear $P(k)$ computed with the halo model is certainly not accurate at small scales; second Σ is computed assuming linearity. Hence a more consistent approach would be to limit ourselves to less nonlinear scales. We have therefore built alternative WL Fisher matrices using $k_{\rm max} = 0.5 h$ Mpc^{-1}, which corresponds to $\ell_{\rm max} \simeq 30$ and falls less deeply into the nonlinear regime. The results are shown in Fig. 5. Here, apart from realizing that the forecasted errors become slightly larger (due to the fact that we use less information), we notice something interesting: the degeneracy has weakened considerably. The reason for this can probably be found by looking again at Fig. 1: at larger scales (corresponding to smaller ℓ) the derivatives of Q with respect to c_s^2 and c_v^2 start to differ from those of Σ. Hence, since for Fig. 1 we used a smaller number of the ℓs falling into the interval where $\partial\Sigma/\partial X \simeq \partial Q/\partial X$, the total result is less degenerate. In particular, in this case we can fully trust the results shown in the middle and lower panels of the aforementioned figure. Looking at Fig. 1 we can also understand another reason why removing so many ℓs from our Fisher matrix calculation does not make errors on c_s^2 and c_v^2 much larger, but they stay of the same order of magnitude (apart from the case $c_s^2 = c_v^2 = 10^{-6}$); compare Fig. 4 with Fig. 5. We see from Fig. 1 that the scales most sensitive to c_s^2 and c_v^2 (i.e. those where the derivatives have the largest amplitude) are those around $k \sim 0.01$. Below $k \sim 0.1$ there is little contribution, and this is due to the fact that dark energy perturbations are suppressed on small scales.

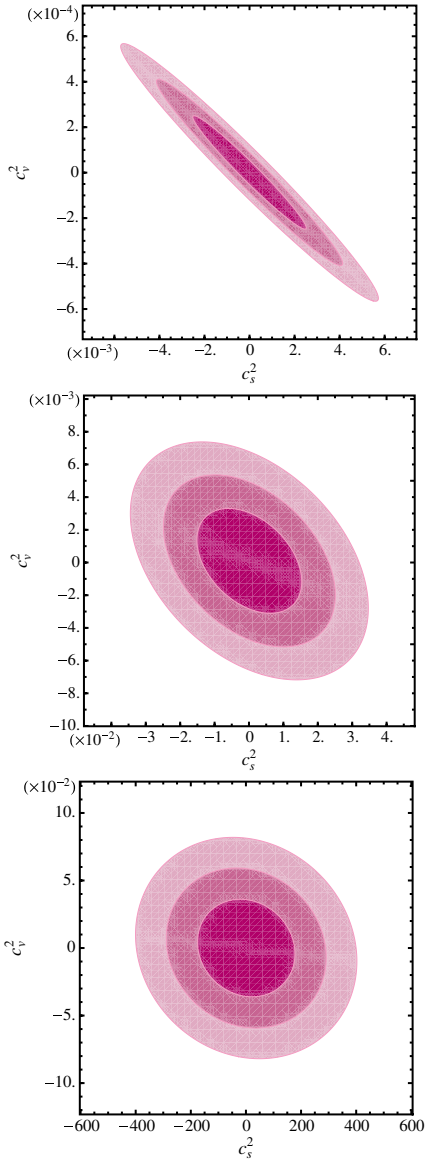FIG. 5 (color online). Same as Fig. 4 but using only scales closer to linearity, with $\ell_{\max} = 30$, which corresponds to $k_{\max} = 0.5h/\text{Mpc}^{-1}$. We notice that the degeneracy between c_s^2 and c_v^2 of Fig. 4 is removed, strongly for the cases of the two lowest panels. This is due to the fact that at larger scales the parameters Σ and Q start carrying information on both c_s^2 and c_v^2 and not only on a unique combination of them (c_{eff}^2). The worsening of errors due to the use of a much smaller number of ℓs is not strong due to the fact that at smaller scales our observable is less sensitive to speed of sound and viscosity because here dark energy perturbations are suppressed.

It is fair to make a final important remark: all the results we obtained depend on the parametrization we have used where the effects of the sound speed and the viscosity appear linearly in a unique expression, Eq. (16). This implies in particular that it may be possible that a different parametrization of the anisotropic stress removes the aforementioned degeneracy problem.
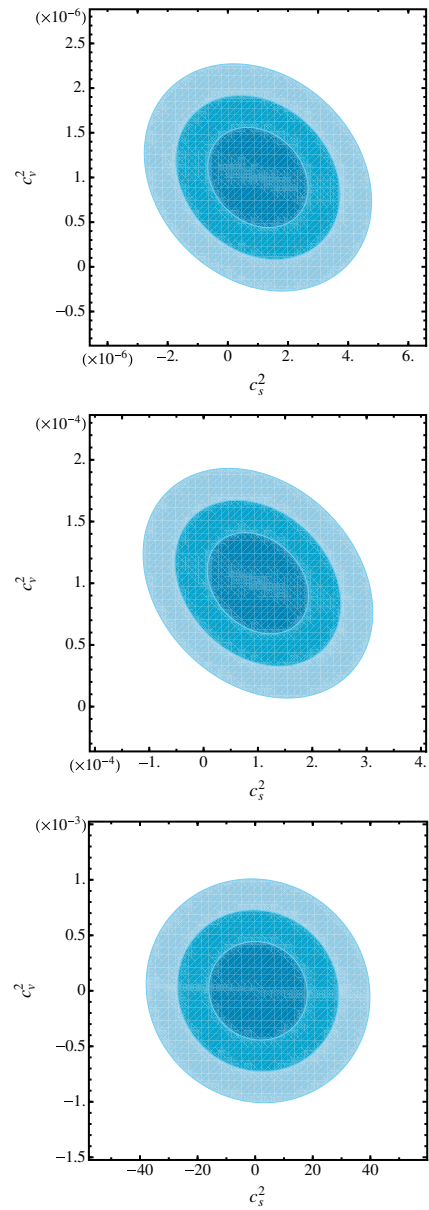
FIG. 6 (color online). Errors on the sound speed and viscosity parameter from the Euclid galaxy redshift survey: 1, 2 and 3σ Fisher ellipses for the parameters c_s^2 and c_v^2. The top panel corresponds to the fiducial $c_s^2 = c_v^2 = 10^{-6}$, the central panel to $c_s^2 = c_v^2 = 10^{-4}$ and the bottom one to the case $c_s^2 = 1$ and $c_v^2 = 10^{-6}$. Here we can see that no degeneracy is present, but errors are again very large, of the order of $\sim 100\%$ in almost all cases (exceptions are $\sigma_{c_v^2} \sim 10\%$ for $c_s^2 = c_v^2 = 10^{-6}$ and $\sigma_{c_v^2} = 1000\%$ for $c_s^2 = 1$, $c_v^2 = 0$).

B. Galaxy clustering

Let us now show and comment on the Fisher matrix forecasts for the Euclid galaxy *redshift* survey, computed for the same three fiducial models previously indicated for the WL case, i.e. $c_s^2 = c_v^2 = 10^{-6}$, $c_s^2 = c_v^2 = 10^{-4}$ and $c_s^2 = 1$ $c_v^2 = 0$.

Following [26] we write the observed galaxy power spectrum as

$$P_{\text{obs}}(z, k_r) = \frac{D_{Ar}^2(z)H(z)}{D_A^2(z)H_r(z)} G^2(z)b(z)^2(1 + \beta\mu^2)^2 P_{0r}(k)$$
$$+ P_{\text{shot}}(z), \qquad (40)$$

where the subscript r refers to the values at which we evaluate the Fisher matrix, i.e. the reference (or fiducial) cosmological model. Here P_{shot} is a scale-independent offset due to imperfect removal of shot noise, μ is the cosine of the angle of the wave mode with respect to the line of sight, P_{0r} is the fiducial matter power spectrum evaluated at redshift zero, $G(z)$ is the linear growth factor of the matter perturbations, $b(z)$ is the bias factor and $D_A(z)$ is the angular diameter distance. The wave number k has also to be written in terms of the fiducial cosmology ([26] and see also [27,28] for more details).

The spectroscopic survey covers a redshift range of $0.65 < z < 2.05$, which we divide into 14 bins of equal width $\Delta z = 0.1$. As regards the bias, we assume it to be scale independent, since this is a quite good approximation for the large linear scales that we will use. Our fiducial bias was derived by [29] using a semianalytical model of galaxy formation, and it is the same bias function used for the Euclid Red Book forecasts. The expected galaxy number densities that we used can be found in [30] and were computed by using a sophisticated simulation [17]. The scales R used are such that $\sigma^2(R) \le 0.25$, with an additional cut at $k_{\text{max}} = 0.20h \text{ Mpc}^{-1}$ to avoid nonlinearity problems.

In the computation of the GC Fisher matrix we do not incur in the same degeneracy problem of the WL survey: our matrices are far from being singular; hence we can safely produce forecasts on the errors on c_s^2 and c_v^2.

The results are shown in Fig. 6, where the 1, 2 and 3σ forecasted contours are shown for all the analyzed cases. In the cases $c_s^2 = c_v^2 = 10^{-6}$ and $c_s^2 = c_v^2 = 10^{-4}$ we notice that the errors on both parameters are best but still of the order of 100% (the only exception is $\sigma_{c_v^2} \sim 10\%$ for $c_s^2 = c_v^2 = 10^{-6}$). In the case where $c_s^2 = 1$ and $c_v^2 = 0$ the error on the sound speed is even larger, i.e. about 1000%.

For a more quantitative insight we list the fully marginalized errors on c_s^2 and c_v^2 in Table III.

C. Combining weak lensing and galaxy clustering

As we have seen previously, it seems that WL data, if one could remove their degeneracy, would provide quite good constraints to speed of sound and viscosity (or at
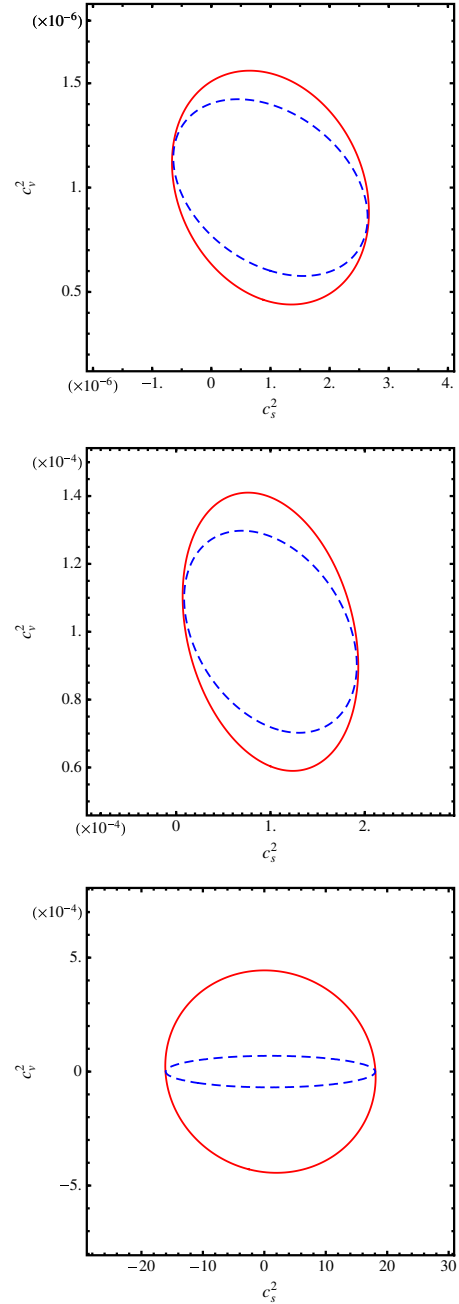
FIG. 7 (color online). Errors on sound speed and viscosity parameter from GC (red solid ellipses), and from the combination GC and WL data (blue dashed ellipses): 1σ Fisher ellipses for the parameters c_s^2 and c_v^2. The top panel corresponds to the fiducial $c_s^2 = c_v^2 = 10^{-6}$, the central panel to $c_s^2 = c_v^2 = 10^{-4}$ and the bottom one to the case $c_s^2 = 1$ and $c_v^2 = 10^{-6}$. The Fisher matrices were produced by neglecting the covariance between WL and GC observations. It can be seen that the addition of WL data visibly improves the constraints, by mostly constraining c_v^2.

TABLE III. Relative errors on the parameters c_s^2 and c_v^2 from the Euclid galaxy redshift survey. For the case $c_v^2 = 0$ the absolute error $\sigma_{c_v^2}$ is given.

		GC	
c_s^2	c_v^2	$\sigma_{c_s^2}/c_s^2$	$\sigma_{c_v^2}/c_v^2$
10^{-6}	10^{-6}	1.10	0.37
10^{-4}	10^{-4}	0.615	0.271
1	0	11.3	$\sigma_{c_v^2} = 2.93 \times 10^{-4}$

TABLE IV. Relative errors on the parameters c_s^2 and c_v^2 from the Euclid survey, including WL and GC data and neglecting correlations between them. For the case $c_v^2 = 0$ the absolute error $\sigma_{c_v^2}$ is given.

WL + GC			
c_s^2	c_v^2	$\sigma_{c_s^2}/c_s^2$	$\sigma_{c_v^2}/c_v^2$
10^{-6}	10^{-6}	1.08	0.28
10^{-4}	10^{-4}	0.604	0.197
1	0	11.3	$\sigma_{c_v^2} = 4.5 \times 10^{-5}$

least not much worse than GC does). Hence adding WL data to GC observations should improve constraints on c_s^2 and c_v^2.

The simplest way to produce forecasts on our combined data sets is to neglect the covariance between WL and galaxy clustering observations. By doing so, we obtain the forecasted error ellipses shown in Fig. 7, where we also show the error ellipses from galaxy clustering only. Here we see that WL observations reduce errors on the two parameters, if not strongly at least visibly. We have already explained earlier why WL observations give degenerate constraints on c_s^2 and c_v^2 when these have very small fiducial values, while the main parameters observed by galaxy clustering are Q and G, which are not as degenerate as Q and Σ. Nevertheless, the reason galaxy clustering observations give the main contribution in constraining c_s^2 and c_v^2, as can be seen by noticing the relatively small improvement in the combined errors in Fig. 7, probably lies only in the properties of the survey, and most likely the very small redshift error has a big role in this too.

When combining GC data to the more conservative WL data (computed using $k_{max} = 0.5h/$Mpc), the latter do not improve constraints. For this reason it will be very important in the future to build a reliable model for the nonlinear regime, both for the standard ΛCDM model and for our imperfect fluid model.

We summarize the result of joining WL and GC data on the fully marginalized errors on c_s^2 and c_v^2 in Table IV.

A final remark to close this section: to produce a more accurate forecast of how the combination of WL and GC data will affect errors on c_s^2 and c_v^2, we would need to evaluate accurately the covariance between the two data sets. Although the number of galaxies observed spectroscopically is only $\sim 1/4$ of those observed photometrically, and we do not expect covariance to be very large, it could affect the estimate. This is left for future work.

V. MODEL COMPARISON

To understand more quantitatively whether Euclid will be able to distinguish viscous dark energy from other less exotic models, we estimate in this section the expected Bayesian evidence, which gives a measure of the probability of one model with respect to the other.

The Bayes' factor B_{12} of models $\mathcal{M}_1$ and $\mathcal{M}_2$ is defined as the ratio of the model likelihoods through (see [31])

$$\frac{p(\mathcal{M}_1|d)}{p(\mathcal{M}_2|d)} = \frac{\pi(\mathcal{M}_1)}{\pi(\mathcal{M}_2)} B_{12}, \tag{41}$$

where $p(\mathcal{M}_i|d)$ is the normalized posterior probability distribution of $\mathcal{M}_i$ and $\pi(\mathcal{M}_i)$ is the prior probability distribution for the model. If we do not have any reason to prefer one model over the other before we see the data, then $\pi(\mathcal{M}_1) = \pi(\mathcal{M}_2) = 1/2$ and

$$B_{12} = \frac{p(\mathcal{M}_1|d)}{p(\mathcal{M}_2|d)}. \tag{42}$$

In the case of nested models, i.e. when $\mathcal{M}_1$ can be obtained from $\mathcal{M}_2$ by fixing the parameter(s) ω to $\omega*$, the expression of B_{12} can be simplified to give the Savage-Dickey density ratio (SDDR); see e.g. [32]:

$$B_{12}^{\text{SDDR}} = \frac{p(\omega|d, \mathcal{M}_2)}{\pi(\omega|\mathcal{M}_2)} \bigg|_{\omega=\omega^*}, \tag{43}$$

where $p(\omega|d, \mathcal{M}_2)$ is the normalized posterior probability distribution and $\pi(\omega|\mathcal{M}_2)$ is the prior probability distribution for the parameter ω of model $\mathcal{M}_2$, marginalized over all other parameters.

The ratio of the model probabilities can be interpreted as "betting odds," and since we set the prior probabilities of all models equal, the same is true for the Bayes factors between models. It then makes sense to use the logarithm of the Bayes factor, which we will call the Bayesian evidence,

$$\mathcal{E} = \ln B_{12}. \tag{44}$$

We will use the interpretation of $\mathcal{E}$ in terms of Jeffrey's scale [33] as given in [32]: The evidence of one model against another one is denoted as not significant, substantial, strong or decisive when $|\mathcal{E}|$ is <1, 1–2.5, 2.5–5 and >5, respectively.

To understand whether a positive viscosity can be distinguished from no viscosity by our data, let us take as our model $\mathcal{M}_1$ a k-essence fluid, i.e. a dark energy model where the sound speed is a free parameter. Hence we will have free c_s^2 while having fixed c_v^{*2} to zero. Our model $\mathcal{M}_2$ will be instead the full viscous dark energy model. For $\mathcal{M}_2$'s extra parameter c_v^2, we choose a flat prior $\pi(c_v^2|\mathcal{M}_2)$ in the range $0 \leq c_s^2 \leq 1$, and $\mathcal{M}_1$ is nested in $\mathcal{M}_2$ at $c_v^2 = 0$. The motivation for choosing a positive value for c_v^2 is to avoid instabilities in the solution for the anisotropic stress function (see [10] for a more detailed explanation). As our likelihood function we take the one forecasted with the Fisher matrix method: $p(d|x_i, \mathcal{M}_2) \propto \exp\left[-1/2(x_i - \bar{x}_i)^T F_{x_i x_j}(x_j - \bar{x}_j)\right]$, where $\bar{x}_i$ is the fiducial value of parameter x_i. We marginalize the likelihood function $p(d|x_i, \mathcal{M}_2)$ over all possible values of c_s^2 so that we obtain

$$p(d|c_v^2, \mathcal{M}_2) = \frac{1}{N} \exp\left[-\frac{1}{2}\left(\frac{c_v^2 - \bar{c}_v^2}{\sigma_{c_v^2}}\right)^2\right], \quad (45)$$

where $\sigma_{c_v^2}$ is estimated with the Fisher matrix: $\sigma_{c_v^2} = (F^{-1})_{c_v^2 c_v^2}$ and the normalization constant of the likelihood is $N = \sqrt{2\pi}\sigma_{c_v^2}$. Our posterior $p(c_v^2|d, \mathcal{M}_2) \propto p(d|c_v^2, \mathcal{M}_2)\pi(c_v^2|\mathcal{M}_2)$ is hence nonzero only in the interval $0 \leq c_v^2 \leq 1$, where it is given by

$$p(c_v^2|d, \mathcal{M}_2) = \frac{1}{N'} \exp\left[-\frac{1}{2}\left(\frac{c_v^2 - \bar{c}_v^2}{\sigma_{c_v^2}}\right)^2\right], \quad (46)$$

where the normalization constant N' is computed by integrating $p(c_v^2|d, \mathcal{M}_2)$ over the interval $0 \leq c_v^2 \leq 1$. The Bayesian evidence is therefore

$$\mathcal{E} \equiv \ln B_{12} = \ln \frac{\Delta c_v^2}{N'} - \frac{1}{2}\left(\frac{c_v^{*2} - \bar{c}_v^2}{\sigma_{c_v^2}}\right)^2, \quad (47)$$

where Δc_v^2 is the interval in c_v^2 allowed by the flat prior, so that $\Delta c_v^2 = 1$ in our case. Let us understand in detail the meaning of this equation. A positive $\mathcal{E}$ will indicate evidence in favor of $\mathcal{M}_1$, i.e. k-essence, while a negative $\mathcal{E}$ will correspond to evidence in favor of $\mathcal{M}_2$, i.e. viscous dark energy. $|\mathcal{E}|$ indicates the strength of this evidence and can be compared to Jeffreys' scale, as explained above. The term $-(1/2)(c_v^{*2} - \bar{c}_v^2)^2/\sigma_{c_v^2}^2$ measures the distance between the model with posterior mean $\bar{c}_v^2$, in our case the chosen fiducial c_v^2, and the simpler model, in our case k-essence ($c_v^{*2} = 0$). We see that this term is always negative, meaning that it contributes evidence in favor of model $\mathcal{M}_2$. It accounts for the fact that the "true" (fiducial) model is fitting the data better (by construction in our case). The term $\ln \Delta c_v^2/N'$ measures the ratio of the area of the c_v^2 parameter space allowed by the more complex model to the area of the error ellipse. It represents therefore the "Occam razor" term, disfavoring too complex models that "waste" too much of the prior space. Since in our case $\ln \Delta c_v^2 = 0$, we are left with the term $-\ln N'$. This is the only term that can push the evidence toward positive values, in favor of model $\mathcal{M}_1$, i.e. k-essence. When the simpler model is favored, it means that the improvement gained by having a better fit to the data is not compensating for the increased complexity of the model.

Our results are summarized in Table V. We notice that the only case where there is (strong) evidence in favor of viscous dark energy corresponds to the choice of posterior mean $\bar{c}_s^2 = \bar{c}_v^2 = 10^{-4}$ and to the use of both WL and GC. In all the other cases the simpler k-essence is favored, so Euclid data alone are not enough to allow a detection of viscosity. An important reason for this result comes from our choice of prior, which implies that we would have expected to measure any c_v^2 between 0 and 1 with equal probability. When the data favor a c_v^2 very close to zero, then Occam's razor indicates that exactly zero is the better answer. Overcoming this effect then requires a highly

TABLE V. Bayesian evidence, $\ln B_{12}$, for the models $\mathcal{M}_1$ and $\mathcal{M}_2$, where $\mathcal{M}_1$ is a fluid k-essence model, with c_s^2 allowed to vary and no viscosity, while $\mathcal{M}_2$ is a viscous dark energy model. We compute $\ln B_{12}$ for different posterior means $\bar{c}_s^2$ and $\bar{c}_v^2$.

Bayesian evidence $\mathcal{E} = \ln B_{12}$		
$\mathcal{M}_1$: fluid k-essence (variable c_s^2, $c_v^2 = 0$)		
$\bar{c}_s^2 = 1\ \bar{c}_v^2 = 0$	$\bar{c}_s^2 = \bar{c}_v^2 = 10^{-4}$	$\bar{c}_s^2 = \bar{c}_v^2 = 10^{-6}$
GC — 7.9	2.8	10.2
GC + WL — 9.8	−3.0	7.8

significant detection of $c_v^2 \neq 0$. Of course in the case where the fiducial model has zero viscosity necessarily the simpler model is always favored, and having more data strengthens its evidence.

The effect of the prior is shown in Fig. 8, where the black thin (red thick) lines indicate the case where the fiducial (true) model has $\bar{c}_v^2 = \bar{c}_s^2 = 10^{-6}$ ($\bar{c}_v^2 = \bar{c}_s^2 = 10^{-4}$). Solid

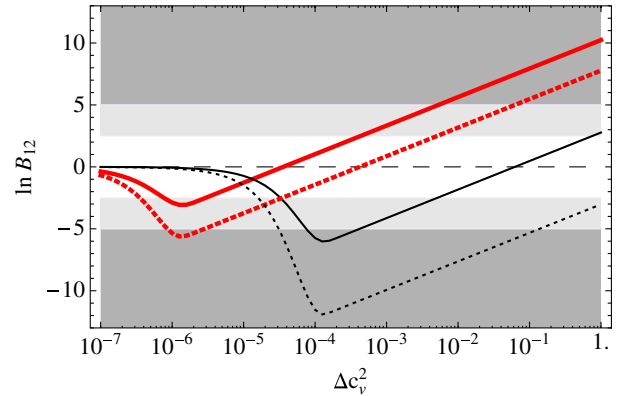

FIG. 8 (color online). Bayesian evidence, $\ln B_{12}$, for the models $\mathcal{M}_1$ (a k-essence fluid with arbitrary constant sound speed c_s^2) and $\mathcal{M}_2$ (viscous dark energy), as a function of c_v^2, i.e. the range in c_v^2 allowed by our (flat) prior: $\Delta c_v^2 = c_{v,\max}^2 - c_{v,\min}^2$, where we fix $c_{v,\max}^2$ to 0. The black thin (red thick) lines represent the case where the fiducial model (also best fit of the posterior) is $\bar{c}_v^2 = \bar{c}_s^2 = 10^{-4}$ ($\bar{c}_v^2 = \bar{c}_s^2 = 10^{-6}$). The solid (dashed) lines indicate the use of GC (GC and WL) data. The darker (lighter) shaded regions correspond to decisive (strong) evidence in favor of viscous DE (where $\ln B_{12} < 0$) or k-essence (where $\ln B_{12} > 0$). We see that the evidence in favor of viscous DE increases until the $c_{v,\max}^2$ of the prior reaches a value of the order of the fiducial c_v^2 considered, and then decreases as the log of Δc_v^2, reaching eventually evidence in favor of k-essence. In the case of using only GC data, we see that when choosing $\bar{c}_v^2 = \bar{c}_s^2 = 10^{-6}$, it is not possible to reach decisive but only strong evidence, while when $\bar{c}_v^2 = \bar{c}_s^2 = 10^{-4}$ decisive evidence is reached when $\Delta c_v^2 \simeq 10^{-4}$. Adding WL data allows also decisive evidence in favor of the model with $\bar{c}_v^2 = \bar{c}_s^2 = 10^{-6}$ to be reached (if $\Delta c_v^2 \simeq 10^{-6}$). Also, using joint GC and WL data, decisive evidence in favor of the viscous DE model with $\bar{c}_v^2 = \bar{c}_s^2 = 10^{-4}$ is reached for any prior having Δc_v^2 between 2×10^{-5} and 10^{-1}.

(dashed) lines represent the use of GC (GC and WL) data. Here we notice that, as we expect, when the range of the flat prior is of the order of the fiducial value of c_v^2, then we obtain the maximal evidence in favor of the viscous DE model. As soon as the interval allowed by the prior becomes much larger than the expected value for c_v^2, the more complex model is disfavored as it wastes too much prior space, and the evidence in favor of the simpler k-essence model starts growing (as the log of Δc_v^2) until the k-essence model becomes favored. In particular we see that, when using both GC and WL, the evidence in favor of viscous DE becomes decisive in the case $\bar{c}_v^2 = \bar{c}_s^2 = 10^{-4}$ if the prior is $2 \times 10^{-5} \lesssim \Delta c_v^2 \lesssim 10^{-1}$, in the case $\bar{c}_v^2 = \bar{c}_s^2 = 10^{-6}$ only in the narrower range $8 \times 10^{-7} \lesssim \Delta c_v^2 \lesssim 2 \times 10^{-6}$. We finally note that if the prior range is much smaller than the fiducial value, then the posterior (which is limited by the prior) becomes flatter and flatter so that the Bayes factor converges toward unity for very small priors.

We could also have compared standard quintessence ($c_s^2 = 1$ and $c_v^2 = 0$) to our viscous dark energy model. However, for all cases with small sound speeds we would have obtained a very decisive evidence in favor of viscous dark energy—but the result would have been driven by the detection of a sound speed different from the speed of light, rather than by a nonzero viscosity: as shown in [20], it is possible to clearly distinguish the true sound speed from $c_s = 1$ for $c_s \lesssim 10^{-2}$ even in the absence of viscosity (at least for our choice of $w = -0.8$). The use of k-essence as the comparison model allows one to focus exclusively on the question whether a nonzero viscosity could be detected.

VI. CONCLUSIONS

In this work we have studied how well a viscous dark energy model can be constrained by the Euclid weak lensing and galaxy clustering surveys.

The model was first proposed by [11] to describe a fluid with anisotropic stress due to viscosity. It can reproduce the neutrino anisotropy up to the quadrupole, and setting the anisotropy parameter c_v^2 to zero reduces it to the standard case of no viscosity. Our dark energy imperfect fluid is hence parametrized by c_v^2, together with the speed of sound and the background equation of state.

The Euclid survey is in principle particularly apt to constrain our model because—through both its WL and galaxy 3D power spectrum probes—it measures, together with the background expansion, also the metric perturbations, which is essential to constrain perturbation quantities such as the viscosity and the speed of sound.

As regards WL, before forecasting the errors with the Fisher matrix technique, we have analyzed the WL power spectrum. We have found that it constrains the clustering parameter Q, the WL potential Σ and the growth factor G. Of these, the most sensitive to c_s^2 and c_v^2 are Σ and Q. For very small values of the speed of sound and the viscosity, their dependence on these parameters is identical at most

scales. This generates a problem for WL constraints, as they will be almost completely degenerate. This is evident once we compute the forecasted errors. We do this for three fiducial models: $c_s^2 = c_v^2 = 10^{-6}$, $c_s^2 = c_v^2 = 10^{-4}$ and $c_s^2 = 1$ $c_v^2 = 0$ but due to the degeneracy problem the only reliable errors are those computed for the last case and amount to $\sigma_{c_s^2} = 201$, $\sigma_{c_v^2} = 1.55 \times 10^{-2}$. The previous results correspond to the optimistic case of having a reliable model for the nonlinear modes up to $\ell = 5000$. If we use the more realistic limiting $\ell = 30$, the degeneracy is weakened—because fewer of the degenerate scales are used—and we can also trust results for the case $c_s^2 = c_v^2 = 10^{-4}$, but the errors get even worse.

As regards the galaxy power spectrum, it constrains Q, G and the growth rate f through redshift space distortions. The most sensitive parameters to the speed of sound and the viscosity are here Q and G, and, contrary to the WL case, there is no degeneracy problem. Using the Fisher matrix method, we forecast errors on our model's parameters. They are of the order of 100% for both c_s^2 and c_v^2 for the fiducial models $c_s^2 = c_v^2 = 10^{-6}$ and $c_s^2 = c_v^2 = 10^{-4}$, while they are of about 1000% on c_s^2 for the fiducial case $c_s^2 = 1$, $c_v^2 = 0$.

If we combine the optimistic WL forecast and GC constraints (assuming no covariance between these data), we improve visibly our results, while when adding the more pessimistic WL case to galaxy power spectrum constraints are left almost unchanged.

To quantify the ability of Euclid to distinguish viscous dark energy from models with no viscosity, we evaluate the Bayesian evidence and find that for the fiducial model with $c_s^2 = c_v^2 = 10^{-4}$ the joint GC and WL survey will be able to provide strong evidence in favor of viscosity, while in all other cases the higher complexity of the model is not compensated by a better fit to the data. This is partially due to our choice of uniform prior on c_v^2 in the range [0,1]. If we relax this assumption, we find that it is possible to obtain decisive evidence in favor of viscous DE even with GC data alone if the range of c_v^2 allowed by the prior is of the order of the fiducial c_v^2, and for a wider choice of prior range when using both GC and WL data and for the case $\bar{c}_v^2 = \bar{c}_s^2 = 10^{-4}$.

Summarizing, future galaxy surveys like Euclid will be only marginally able to constrain viscous dark energy models. This statement depends of course on the model being analyzed. Some modified gravity models have a larger effective anisotropic stress than the viscous dark energy models considered here, and Euclid may have a better chance at detecting a nonzero σ in this case. Alternatively one could combine Euclid with other observations such as the cosmic microwave background, cluster counts, data from type-Ia supernovae and measurements of the integrated Sachs-Wolfe effect: all these observables constrain themselves c_s^2 and c_v^2 and/or reduce the errors on background parameters and therefore reduce also

marginalized errors on perturbation quantities. These interesting developments are left to future work.

ACKNOWLEDGMENTS

[1] A. G. Riess *et al.*, Astron. J. **116,** 1009 (1998).
[2] S. Perlmutter *et al.*, Astrophys. J. **517,** 565 (1999).
[3] D. Sapone, Int. J. Mod. Phys. A **25,** 5253 (2010).
[4] M. Kunz, C.R. Phys. **13,** 539 (2012).
[5] L. Amendola and S. Tsujikawa, *Dark Energy: Theory and Observations* (Cambridge University Press, Cambridge, 2010).
[6] S. M. Carroll, Living Rev. Relativity **4,** 1 (2001).
[7] G. R. Dvali, G. Gabadadze, and M. Porrati, Phys. Lett. B **484,** 112 (2000).
[8] C. de Rham, S. Hofmann, J. Khoury, and A. J. Tolley, J. Cosmol. Astropart. Phys. 02 (2008) 011; O. Corradini, K. Koyama, and G. Tasinato, Phys. Rev. D **77,** 084006 (2008).
[9] Y. Aghababaie, C. P. Burgess, S. L. Parameswaran, and F. Quevedo, Nucl. Phys. **B680,** 389 (2004); C. P. Burgess and L. van Nierop, Phys. Dark Univ. **2,** 1 (2013); C. P. Burgess, L. van Nierop, S. Parameswaran, A. Salvio, and M. Williams, J. High Energy Phys. 02 (2013) 120; A. Salvio, J. Phys. Conf. Ser. **437,** 012004 (2013); M. Williams, C. P. Burgess, L. van Nierop, and A. Salvio, J. High Energy Phys. 01 (2013) 102.
[10] D. Sapone and E. Majerotto, Phys. Rev. D **85,** 123529 (2012).
[11] W. Hu, Astrophys. J. **506,** 485 (1998).
[12] T. Koivisto and D. F. Mota, Phys. Rev. D **73,** 083502 (2006).
[13] D. F. Mota, J. R. Kristiansen, T. Koivisto, and N. E. Groeneboom, Mon. Not. R. Astron. Soc. **382,** 793 (2007).
[14] D. Sapone and M. Kunz, Phys. Rev. D **80,** 083519 (2009).
[15] E. Calabrese, R. de Putter, D. Huterer, E. V. Linder, and A. Melchiorri, Phys. Rev. D **83,** 023011 (2011); M. Archidiacono, E. Calabrese, and A. Melchiorri, Phys. Rev. D **84,** 123008 (2011); G. Ballesteros, L. Hollenstein, R. K. Jain, and M. Kunz, J. Cosmol. Astropart. Phys. 05 (2012) 038; L. Pogosian, A. Silvestri, K. Koyama, and G.-B. Zhao, Phys. Rev. D **81,** 104023 (2010); A. Silvestri, Nucl. Phys. B Proc. Suppl. **194,** 326 (2009).
[16] R. Laureijs *et al.*, arXiv:0912.0914.
[17] R. Laureijs *et al.*, arXiv:1110.3193.
[18] L. Amendola, M. Kunz, and D. Sapone, J. Cosmol. Astropart. Phys. 04 (2008) 013.
[19] E. V. Linder and R. N. Cahn, Astropart. Phys. **28,** 481 (2007).
[20] D. Sapone, M. Kunz, and L. Amendola, Phys. Rev. D **82,** 103535 (2010).
[21] N. Kaiser, Mon. Not. R. Astron. Soc. **227,** 1 (1987).
[22] L. Amendola, M. Kunz, M. Motta, I. D. Saltas, and I. Sawicki, Phys. Rev. D **87,** 023501 (2013).
[23] A. Lewis, A. Challinor, and A. Lasenby, Astrophys. J. **538,** 473 (2000).
[24] A. Amara and A. Refregier, Mon. Not. R. Astron. Soc. **381,** 1018 (2007).
[25] A. Albrecht *et al.*, arXiv:0901.0721.
[26] H. J. Seo and D. J. Eisenstein, Astrophys. J. **598,** 720 (2003).
[27] L. Amendola, C. Quercellini, and E. Giallongo, Mon. Not. R. Astron. Soc. **357,** 429 (2005).
[28] D. Sapone and L. Amendola, arXiv:0709.2792.
[29] A. Orsi, C. M. Baugh, C. G. Lacey, A. Cimatti, Y. Wang, and G. Zamorani, arXiv:0911.0669.
[30] E. Majerotto *et al.*, Mon. Not. R. Astron. Soc. **424,** 1392 (2012).
[31] M. Kunz, R. Trotta, and D. Parkinson, Phys. Rev. D **74,** 023503 (2006).
[32] R. Trotta, Mon. Not. R. Astron. Soc. **378,** 72 (2007).
[33] H. Jeffreys, *The Theory of Probability*, Oxford Classic Texts in the Physical Sciences (Oxford University Press, New York, 1998), 3rd. ed.